

Supplementary Materials for
Macrophages orchestrate the expansion of a proangiogenic perivascular niche during cancer progression

James W. Opzoomer, Joanne E. Anstee, Isaac Dean, Emily J. Hill, Ihssane Bouybayoune, Jonathan Caron, Tamara Muliaditan, Peter Gordon, Dominika Sosnowska, Rosamond Nuamah, Sarah E. Pinder, Tony Ng, Francesco Dazzi, Shahram Kordasti, David R. Withers, Toby Lawrence, James N. Arnold*

*Corresponding author. Email: james.n.arnold@kcl.ac.uk

Published 3 November 2021, *Sci. Adv.* 7, eabg9518 (2021)
DOI: 10.1126/sciadv.abg9518

This PDF file includes:

Legends for tables S1 to S5
Figs. S1 to S6

Other Supplementary Material for this manuscript includes the following:

Tables S1 to S5

Auxiliary Supplementary Tables

Table S1. List of up regulated genes for scRNA-seq TAM clusters versus all other clusters.

Table S2. List of up regulated genes for scRNA-seq TAM clusters TAM06 versus TAM07.

Table S3. List of up regulated genes for facs-sorted bulk RNA-seq of CD45⁻ stromal populations versus all other CD45⁻ stromal populations.

Table S4. List of CellPhoneDB ligand-receptor interactions between perivascular niche cell populations with mean values for ligand-receptor interactions.

Table S5. List of putative growth factor ligand-receptor interactions derived from CellPhoneDB data with relative gene expression.

Supplementary Figures

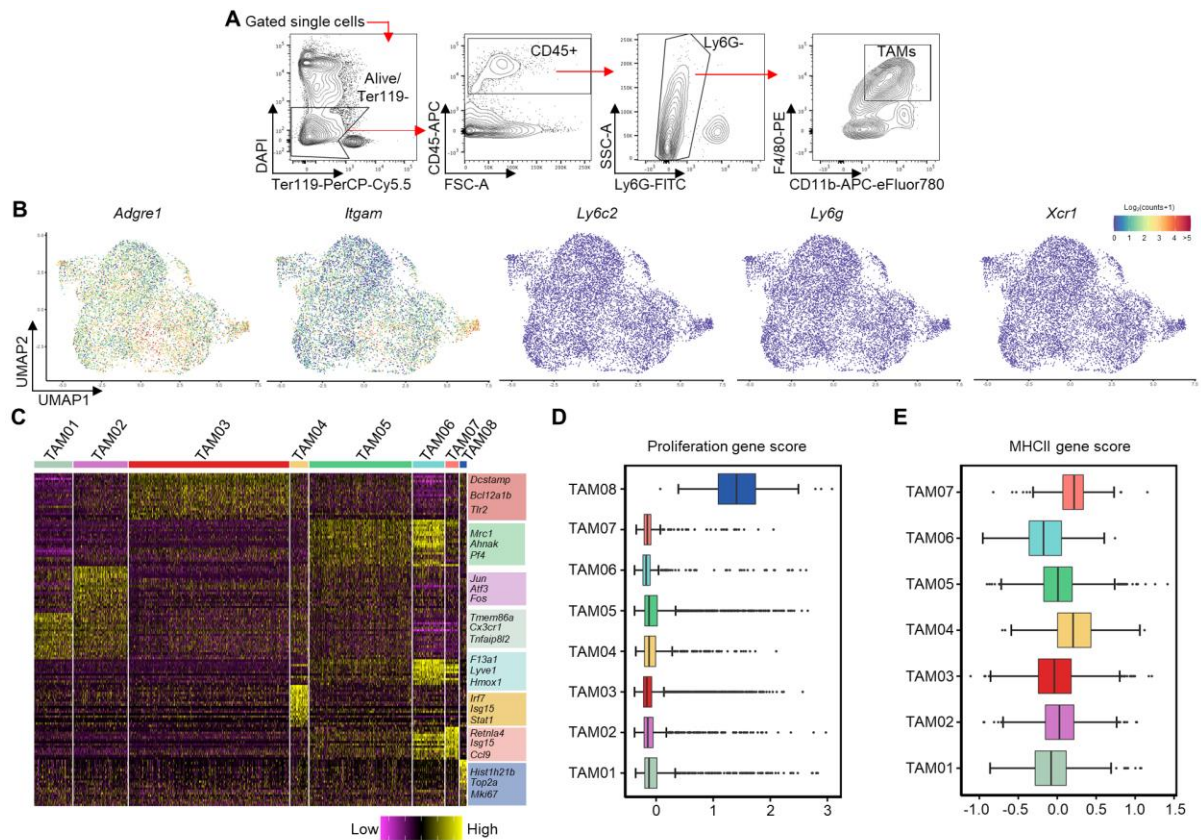


Figure S1. scRNA-seq of TAMs identifies distinct polarization states within the tumor microenvironment. (A) Representative gating strategy for live (7AAD⁻) TAMs for sorting using the indicated surface markers from enzyme-dispersed *MMTV-PYMT* tumors used in scRNA-seq sample preparation analyzed in Fig. 1 and 2. (B) UMAP plots of the 9,039 TAMs sequenced using the 10X Genomics' Chromium platform across n=3 tumors displaying the expression of marker genes used to isolate TAM single cells in (A). (C) Heatmap showing top differentially expressed genes within each TAM cluster shown in Fig.1b, selected genes for each cluster are highlighted to the right of the heatmap. (D,E) Gene scores across all TAM clusters for proliferation (D) and MHCII associated genes (E). Box and whisker plots, the boxes show median and upper and lower quartiles and whiskers shows the largest value no more than 1.5*IQR of the respective upper and lower hinges, outliers beyond the end of the whisker are plotted as individual dots.

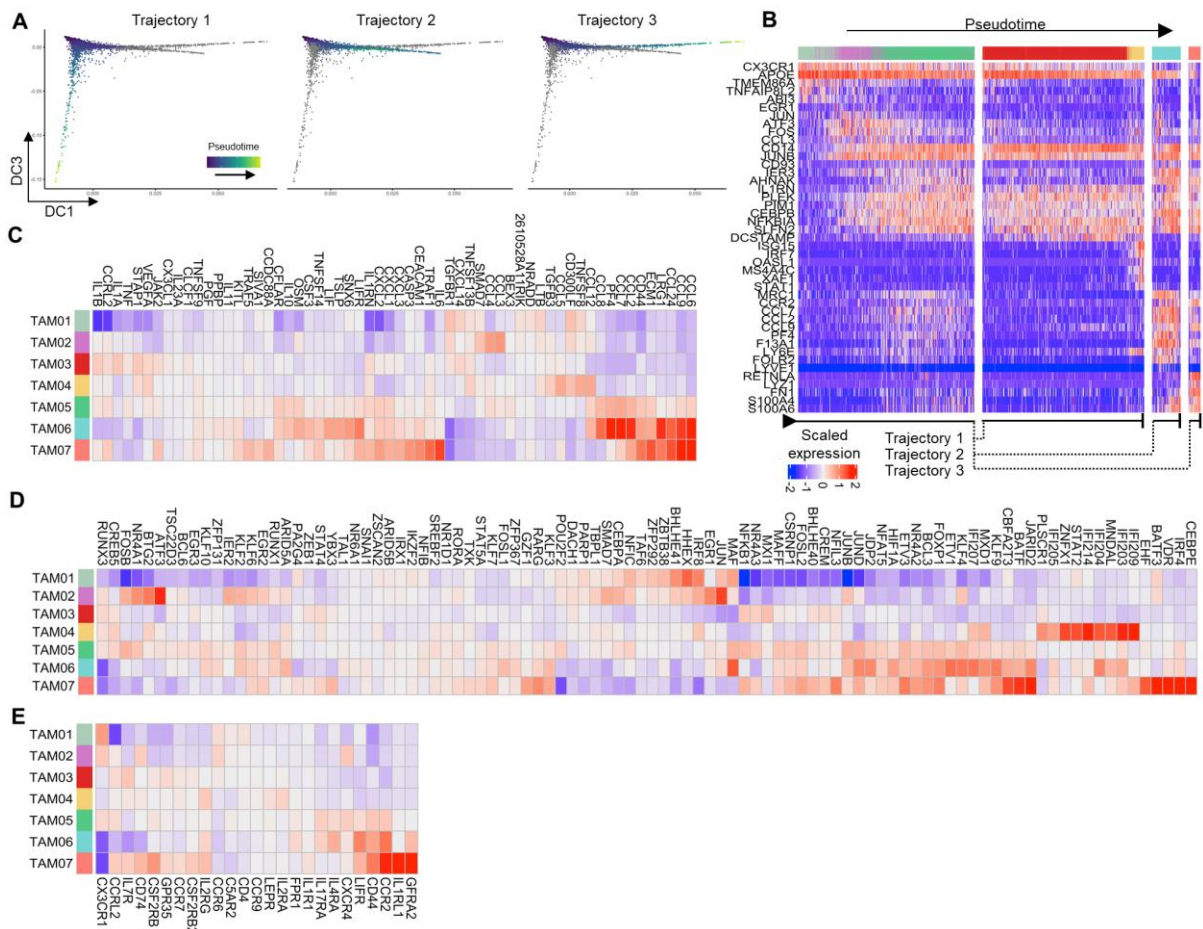


Figure S2. Trajectory analysis of scRNA-seq of TAMs reveals polarization-specific transcription factors and cytokine signatures associated with transcriptomic state. (A) Diffusion component (DC) plot showing single cells colored by pseudotime value for each distinct trajectory predicted by *Slingshot* trajectory analysis. Cells that are not associated with a given trajectory are greyed out. (B) Heatmap of selected genes varying significantly across trajectory. Single cells (columns) are arranged left to right by pseudotime value within their labeled trajectories, branching points are indicated beneath the heatmap. (C-E) Heatmaps representing chemokine, cytokine and complement factor genes (C), transcription factor genes (D) and additional chemokine, cytokine and complement receptor genes (E) that vary significantly across the predicted *Slingshot* trajectories.

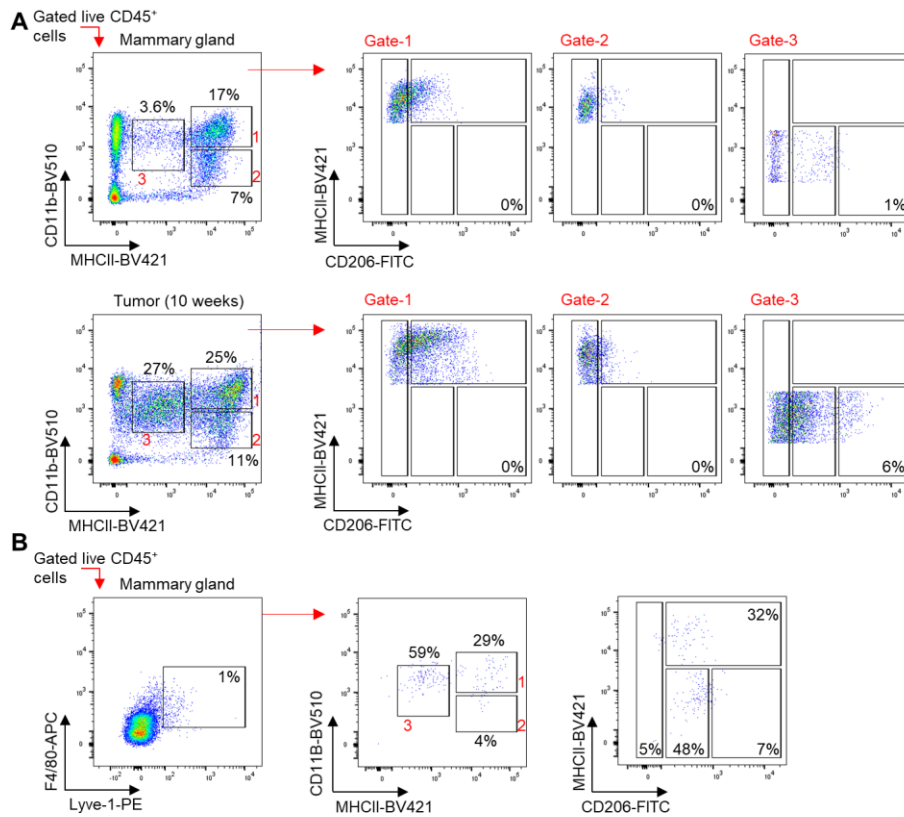


Figure S3. Comparison of macrophage phenotypes in the mammary gland and *MMTV-PyMT* tumors. Representative flow cytometry gating strategy of live (7AAD⁻) CD45⁺ cells assessed according to Franklin et al (35) to resolve macrophage subsets and comparison to those used in the current study. **(A)** Flow cytometry dot plots of enzyme-dispersed tissue from either non-malignant mammary gland (from age-matched PyMT⁻ mice) or *MMTV-PyMT* tumors from 10 week-old mice were stained with antibodies against the indicated markers. Percentage indicated represents the proportion of events falling into the MHCII^{lo} CD206^{hi} gate (where Lyve-1⁺ pVTAMs are identified). **(B)** Dot plots from flow cytometry analysis of enzyme-dispersed tissue from non-malignant mammary gland gating for live (7AAD⁻) CD45⁺ tissue resident Lyve-1⁺ macrophages (left panel) and their distribution for the markers used in **(A)**.

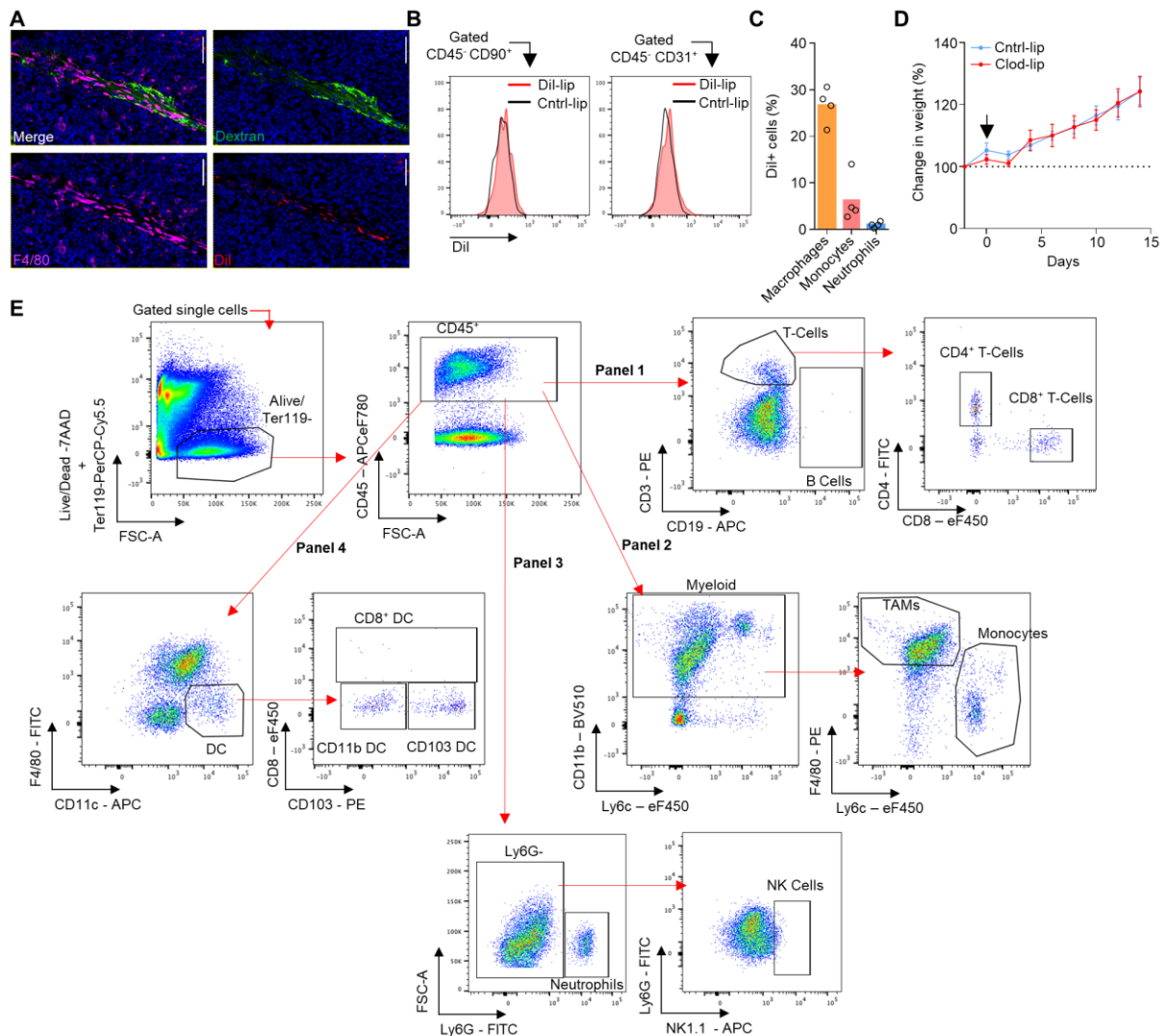


Figure S4. Liposomes are specifically taken up by a PvTAM subset. (A) Representative image of a frozen section of *MMTV-PyMT* tumor showing DAPI (nuclei; blue), i.v. dextran marking vasculature (green), Dil from the liposomes (red) and antibody staining against F4/80 (magenta), scale bar represents 50 μ m. (B) Representative histograms showing Dil-containing liposome uptake (red filled histogram) against PBS-filled liposome treated mice (open black line histogram) in CD90⁺ CAF and CD31⁺ endothelial cells in the CD45⁻ gate of enzyme-dispersed tumors from *MMTV-PyMT* mice treated as shown in Fig. 2J and assessed using flow cytometry, representative of n=3 mice. (C) Proportion of live (7AAD⁻) gated tumor-resident phagocytic populations with detectable Dil uptake as assessed using flow cytometry (n=4 mice). (D-E) Tumor bearing *MMTV-PyMT* mice treated with control PBS-filled liposomes (Cntrl-lip) or clodronate-filled liposomes (Clod-lip) using the treatment regimen shown in Fig. 3A, showing the percentage change in mouse weight over the course of the experiment (D), representative gating strategy for identifying different tumour-resident leukocyte populations in enzyme-dispersed tumors taken at day 15 post initiation of treatment with the respective liposomes (E). Bar charts represent mean and the dots show individual data points from individual tumors and mice. * $P < 0.05$, ** $P < 0.01$.

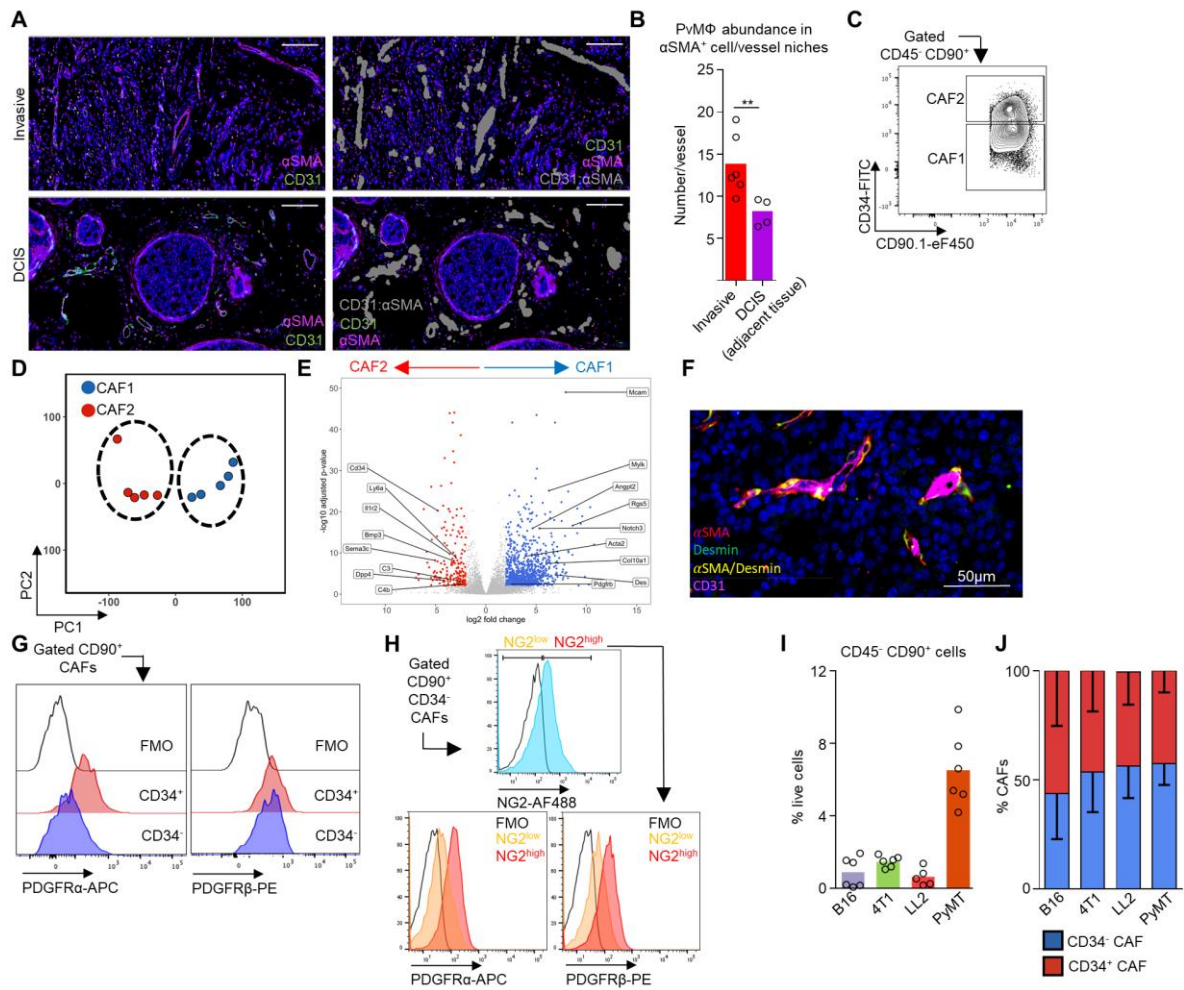


Figure S5. The perivascular niche and mesenchymal cell heterogeneity in murine models of cancer. (A) Representative image of a FFPE section from human invasive ductal mammary carcinoma (top) and DCIS (bottom) stained with DAPI (nuclei; blue) and antibodies against CD31 (green) and α SMA (magenta) where these cells were touching (perivascular niche) cells were labeled grey, CD68 staining events are also displayed on the image, where events less or more than 50 μ m from a vessel labeled orange and yellow respectively. Scale bar indicates 150 μ m. (B) Quantification of the number of CD68⁺ TAMs within the perivascular niche of SMA⁺ stroma touching CD31⁺ vessels (<50 μ m is regarded perivascular) identified from (A), assessed across multiple ROIs (n=6 invasive tumors and n=4 DCIS). (C) Representative gating strategy for flow cytometry sorting the predicted subsets of CAFs by unsupervised clustering analysis. (D-E) Bulk RNA-seq of the CD34⁺/⁻ CAF subsets, showing PCA plot of the bulk-sequenced CAF populations showing the difference in CAF transcriptome (D), differentially expressed genes between CD34⁺/⁻ CAF populations (E) across n=5 tumors and mice. (F) Representative confocal image of a frozen *MMTV-PyMT* tumor section showing DAPI (nuclei; blue), and antibody staining against CD31 (magenta), α SMA (red), desmin (green) and α SMA/desmin co-localization (yellow). Representative of multiple sections from n=4 tumors and mice. Scale bar represents 100 μ m. (G-H) Representative histogram of live (7AAD⁻) CD90⁺CAFs gated using flow cytometry in a representative enzyme-dispersed *MMTV-PyMT* tumor; histogram shows surface staining for the PDGFR α and PDGFR β on CD34⁺/⁻ CAFs (shaded histograms) against that of the fluorescence minus one (FMO) control (open histogram) (G), or gated live (7AAD⁻) CD90⁺CD34⁻ CAFs showing surface staining for NG2 (top; shaded histogram) and the respective expression of PDGFR α and PDGFR β on the CD34⁻ CAFs sub-gated for either 'high' or 'low' surface NG2 expression (bottom; shaded histograms) against that of the FMO control (all; open histograms) (H). (I-J) Mice were injected with the indicated tumor cells and

when tumors reached 1500mm³ they were enzyme-dispersed and analyzed by flow cytometry for the abundance of live (7AAD⁻) CD45⁻CD31⁻CD90⁺ CAFs (**I**) and the relative proportions of CD34⁺ and CD34⁻ CAFs (**J**) across n= 5-6 mice per model. Bar charts represent mean and error bars s.d., dots show individual data points from individual tumors and mice.

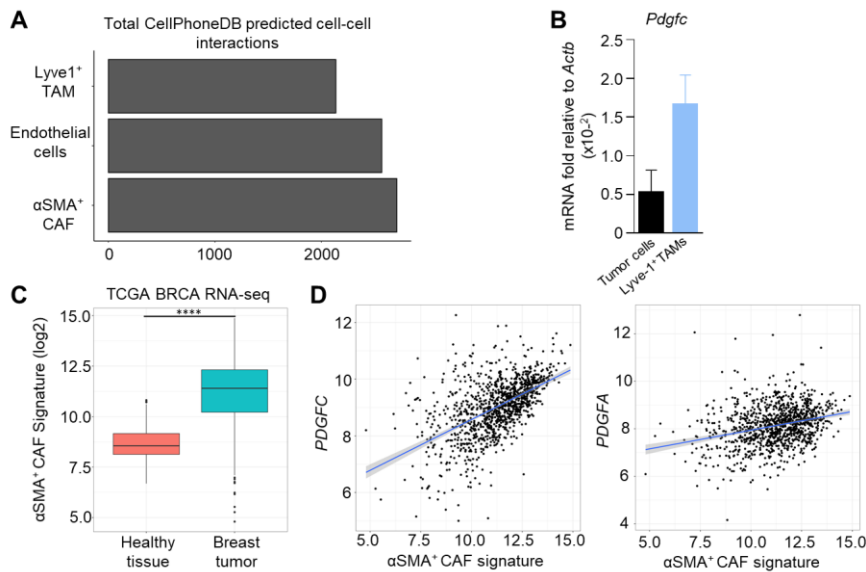


Figure S6. A α SMA⁺ CAF signature correlates with *PDGFC* expression in human breast cancer (**A**) The number of total potential ligand and receptor interactions identified per bulk RNA-sequenced cell type that participate in paracrine and autocrine signaling networks in the perivascular niche. (**B**) *Pdgfc* mRNA expression relative to the housekeeping gene *Actb* in FACS-sorted tumor cells (CD45⁻CD31⁻CD90⁺; n=6) and Lyve-1⁺ TAMs (n=3). (**C**) Normalized log₂ RNA-seq counts for the TCGA-BRCA dataset for the α SMA^{hi} CAF gene signature in non-malignant breast tissue (n=112) and primary breast carcinoma tissue (n=1,093). (**D**) Scatterplot of α SMA⁺ CAF gene signature score (x axis) and *PDGFC* (y axis) (Pearson's r = 0.547, p < 0.0001) (left) or *PDGFA* (y-axis) (Pearson's r = 0.286 p < 0.0001) (right) from the TCGA-BRCA RNA-seq dataset, n=1,093. Box and whisker plots, the boxes show median and upper and lower quartiles and whiskers shows the largest value no more than 1.5*IQR of the respective upper and lower hinges, outliers beyond the end of the whisker are plotted as individual dots. Bar charts represent mean, error bars represent s.e.m. **** P<0.0001.